Global Journal of Researches in Engineering: J
General Engineering
Volume 15 Issue 6 Version 1.0 Year 2015
Type: Double Blind Peer Reviewed International Research Journal
Publisher: Global Journals Inc. (USA)
Online ISSN: 2249-4596 & Print ISSN: 0975-5861

Detection and Parameter Extraction of Low Probability of Intercept Radar Signals using the Hough Transform

By Daniel L. Stevens & Stephanie A. Schuckers

Air Force Research Laboratory Rome, United States

Abstract- Digital intercept receivers are currently moving away from Fourier-based analysis and towards classical time-frequency analysis techniques, such as the Wigner-Ville distribution, Choi-Williams distribution, spectrogram, and scalogram, for the purpose of analyzing low probability of intercept radar signals (e.g. triangular modulated frequency modulated continuous wave and frequency shift keying). Although these classical time-frequency techniques are an improvement over the Fourier-based analysis, they still suffer from a lack of readability, due to cross-term interference, and a mediocre performance in low SNR environments. This lack of readability may lead to inaccurate detection and parameter extraction of these radar signals. In this paper, the use of the Hough transform, because of its ability to suppress cross-term interference, separate signals from cross-terms, and perform well in the presence of noise, is proposed as an improved signal analysis technique. With these qualities, the Hough transform has the potential to produce better readability and consequently, more accurate signal detection and parameter extraction metrics.

Keywords: *radar detection, hough transform, low probability of intercept.*

GJRE-J Classification: *FOR Code: 090609*

Detection and Parameter Extraction of Low Probability of Intercept Radar Signals using the Hough Transform[1]

Daniel L. Stevens α & Stephanie A. Schuckers σ

Abstract- Digital intercept receivers are currently moving away from Fourier-based analysis and towards classical time-frequency analysis techniques, such as the Wigner-Ville distribution, Choi-Williams distribution, spectrogram, and scalogram, for the purpose of analyzing low probability of intercept radar signals (e.g. triangular modulated frequency modulated continuous wave and frequency shift keying). Although these classical time-frequency techniques are an improvement over the Fourier-based analysis, they still suffer from a lack of readability, due to cross-term interference, and a mediocre performance in low SNR environments. This lack of readability may lead to inaccurate detection and parameter extraction of these radar signals. In this paper, the use of the Hough transform, because of its ability to suppress cross-term interference, separate signals from cross-terms, and perform well in the presence of noise, is proposed as an improved signal analysis technique. With these qualities, the Hough transform has the potential to produce better readability and consequently, more accurate signal detection and parameter extraction metrics. Two different triangular modulated frequency modulated continuous wave low probability of intercept radar signals and two different frequency shift keying low probability of intercept radar signals (4-component and 8-component) were analyzed. The following metrics were used for evaluation of the analysis: percent error of chirp rate, percent detection, number of cross-term false positives, and lowest signal-to-noise ratio for signal detection. Experimental results demonstrate that the qualities of suppressing cross-term interference, separating signals from cross-terms, and performing well in a low SNR environment did lead to improved readability over the classical time-frequency analysis techniques, and consequently, provided more accurate signal detection and parameter extraction metrics (smaller percent error from true value) than the classical time-frequency analysis techniques. In addition, the Hough transform was utilized to detect, extract parameters, and properly identify a real-world low probability of intercept radar signal in a low signal-to-noise ratio environment, where the classical time-frequency analysis failed. In summary, this paper provides evidence that the Hough transform has the potential to outperform the classical time-frequency analysis techniques. Future work will include automation of the metrics extraction process, analysis of additional low probability of intercept radar waveforms of interest, and analysis of other real-world low probability of intercept radar signals utilizing more powerful computing platforms.

Keywords: radar detection, hough transform, low probability of intercept.

I. Introduction

In order to perform their functions properly, many of today's radar systems must be able to 'see without being seen' [PAC09], [WIL06]. This necessitates that they be low probability of intercept (LPI) radars. These radars typically have very low peak power, wide bandwidth, high duty cycle, and power management, making them difficult to be detected and characterized by intercept receivers.

Fourier analysis techniques using the FFT have been employed as a tool of the digital intercept receiver for detecting and extracting parameters of LPI radar signals [PAC09]. When a practical non-stationary signal (such as an LPI radar signal) is processed, the Fourier transform cannot efficiently analyze and process the time-varying characteristics of the signal's frequency spectrum, because time and frequency information cannot be combined to tell how the frequency content is changing in time [XIE08], [STE96]. The non-stationary nature of the received radar signal mandates the use of some form of time-frequency analysis for signal detection and parameter extraction [MIL02].

Some of the more common classical time-frequency analysis techniques include the Wigner-Ville distribution (WVD), Choi-Williams distribution (CWD), spectrogram, and scalogram. The WVD exhibits the highest signal energy concentration [WIL06], but has the worse cross-term interference, which can severely limit the readability of a time-frequency representation [GUL07], [STE96], [BOA03]. The CWD is a member of Cohen's class, which adds a smoothing kernel to help reduce cross-term interference [BOA03], [UPP08]. The CWD, as with all members of Cohen's class, is faced with a trade-off between cross-term reduction and time-frequency localization. The Spectrogram is the magnitude squared of the short-time Fourier transform [HLA92], [MIT01]. It has poorer time-frequency localization but less cross-term interference than the

Author α: Air Force Research Laboratory Rome, NY 13441. e-mail: daniel.stevens.7@us.af.mil
Author σ: Department of Electrical and Computer Engineering, Clarkson University Potsdam, NY 13699. e-mail: sschucke@clarkson.edu

[1] Approved for Public Release; Distribution Unlimited: 88ABW-2015-3207 20150624

Global Journal of Researches in Engineering (J) Volume XV Issue VI Version I Year 2015

WVD or CWD, and its cross-terms are limited to regions where the signals overlap [ISI96]. The Scalogram is the magnitude squared of the wavelet transform, and can be used as a time-frequency distribution [COH02], [GAL05], [BOA03]. Like the Spectrogram, the Scalogram has cross-terms that are limited to regions where the signals overlap [ISI96], [HLA92].

Though classical time-frequency analysis techniques, such as those described above, are a great improvement over Fourier analysis techniques, they suffer in general from cross-term interference and a mediocre performance in low SNR environments, as described above. This may result in degraded readability of time-frequency representations, potentially leading to inaccurate LPI radar signal detection and parameter extraction metrics.

A promising avenue for overcoming these shortfalls is the utilization of the Hough Transform, which is very similar to the Radon transform, and is used, for the detection of straight lines and other curves [BAR95], [BEN05], [ZAI99], [INC07]. The Hough transform of a particular time-frequency representation is found by computing the integral of the time-frequency representation along straight lines at different angles. The presence of a 'spike' in the Hough transform representation reveals the presence of high positive values concentrated along a line in the time-frequency representation – whose parameters (such as chirp rate) correspond to the coordinates of the spike (theta and rho values) [BAR92], [YAS06], [BAR95]. Detection can be achieved by establishing a threshold value for the amplitude of the Hough transform spike. Therefore the Hough transform can be used to convert a difficult global detection problem in the time-frequency representation into a more easily solved local peak detection problem in the Hough transform representation.

Since cross-terms have amplitude modulation, the integration implicit in the Hough transform reduces the cross-terms, while the useful contributions, which are always positive, are correctly integrated [TOR07], [BAR92], [BAR95]. Likewise, in the presence of noise, the integration carried out by the Hough transform produces an improvement in SNR [INC07], [YAS06], [NIK08]. These qualities make the Hough transform a viable candidate for analyzing LPI radar signals.

In related work, [WON09] performed research using the WVD followed by the Hough transform as one of their detection and parameter estimation algorithms, but this was utilized for a single chirp signal, which presents no cross-term interference like the triangular modulated FMCW and FSK waveforms that are examined in this paper. [GUL08] utilized the pseudo Wigner-Ville distribution followed by the Radon transform, but used it only for parameter extraction, and not for signal detection. This paper utilized the Hough transform for both parameter extraction and signal detection. [GER09] used an algorithm similar to the WVD followed by the Hough transform, called the periodic Wigner-Ville Hough transform. This algorithm was used on a sawtooth FMCW waveform, which is a viable LPI radar waveform. Their research assumed that phase is coherent from on LFM ramp to the next which is not always the case. Also, for their research, one needed to search for the right repetition period, the right starting frequency and the right slope. Overall, it appears that little research has been done in the area of using the Hough transform for the analysis of triangular modulated FMCW LPI radar signals and FSK LPI radar signals.

In this paper, the Hough transform is evaluated as a technique for improving the readability of the classical time-frequency analysis representations by suppressing cross-term interference, separating signals from cross-terms, and performing well in a low SNR environment. This approach is assessed using 2 triangular modulated FMCW LPI radar signals and 2 FSK LPI radar signals (4-component and 8-component). Metrics designed include: percent error of chirp rate, percent detection, number of cross-term false positives, and lowest SNR for signal detection.

The rest of this paper is organized as follows: Description of the proposed methodology is presented in section II. Experimental results comparing the reassignment method and classical time-frequency analysis techniques are presented in section III, followed by discussion and conclusions.

II. Methodology

The methodologies detailed in this paper describe the processes involved in obtaining and comparing metrics between the classical time-frequency analysis techniques and the Hough transform for the detection and parameter extraction of LPI radar signals.

The tools used for this testing were: MATLAB (version 7.7), Signal Processing Toolbox (version 6.10), Wavelet Toolbox (version 4.3), Image Processing Toolbox (version 6.2), Time-Frequency Toolbox (version 1.0) (http://tftb.nongnu.org/).

All the testing was accomplished on a desktop computer (HP Compaq, 2.5GHz processor, AMD Athlon 64X2 Dual Core Processor 4800+, 2.00GB Memory (RAM), 32 Bit Operating System).

Testing was performed for 4 different waveforms (2 triangular modulated FMCWs and 2 FSKs), each waveform representing a different task (Task 1 through Task 4). For each waveform, parameters were chosen for academic validation of signal processing techniques. Due to computer processing limitations they were not meant to represent real-world values. The number of samples for each test was chosen to be either 256 or 512, which seemed to be the optimum size for the desktop computer. Testing was performed at three different SNR levels: 10dB, 0dB,

Global Journal of Researches in Engineering (J) Volume XV Issue VI Version I Year 2015

and low SNR (the lowest SNR at which the signal could be detected). The noise added was white Gaussian noise, which best reflected the thermal noise present in the IF section of an intercept receiver [PAC09]. Kaiser windowing was used, when windowing was applicable. 25 runs were performed for each test, for statistical purposes. The plots included in this paper were done at a threshold of 5% of the maximum intensity and were linear scale (not dB) of analytic (complex) signals; the color bar represented intensity. The signal processing tools used for each task were:

Classical time-frequency analysis techniques: WVD, CWD, spectrogram, scalogram

Hough transform method: Hough transform of WVD and Hough transform of CWD

Task 1 consisted of analyzing a triangular modulated FMCW signal (most prevalent LPI radar waveform [LIA09]) whose parameters were: sampling frequency=4KHz; carrier frequency=1KHz; modulation bandwidth=500Hz; modulation period=.02sec.

Task 2 was similar to Task 1, but with different parameters: sampling frequency=6KHz; carrier frequency= 1.5KHz; modulation bandwidth=2400Hz; modulation period=.15sec. The different parameters were chosen to see how the different shapes/heights of the triangles of the triangular modulated FMCW would affect the cross-term interference and the metrics.

Task 3 consisted of analyzing an FSK (prevalent in the LPI arena [AMS09]) 4-component signal whose parameters were: sampling frequency=5KHz; carrier frequencies=1KHz, 1.75KHz, 0.75KHz, 1.25KHz; modulation bandwidth=1000Hz; modulation period=.025sec.

Task 4 was similar to Task 3, but for an FSK 8-component signal whose parameters were: sampling frequency=5KHz; carrier frequencies=1.5KHz, 1KHz, 1.25KHz, 1.5KHz, 1.75KHz, 1.25KHz, 0.75KHz, 1KHz; modulation bandwidth=1000Hz; modulation period=.0125sec. The different number of components and different parameters between Task 3 and Task 4 were chosen to see how the different number/lengths of FSK components would affect the cross-term interference and the metrics.

Because of computational complexity, the WVD tests and the Hough transform of WVD tests for 512 samples, SNR=0dB and 512 samples, SNR=low SNR – were not able to be performed for any of the 4 waveforms. It was noted that a single run was still processing after more than 8 hours. The WVD is known to be very computationally complex [MIL02].

After each particular run of each test, metrics were extracted from the time-frequency representation and the Hough transform plot. The metrics extracted were as follows (TF=time-frequency representation; HT=Hough transform):

a) Percent detection

HT: percent of time signal was detected – signal was declared a detection if any portion of each of the signal components exceeded the noise floor threshold (see Figure 1).

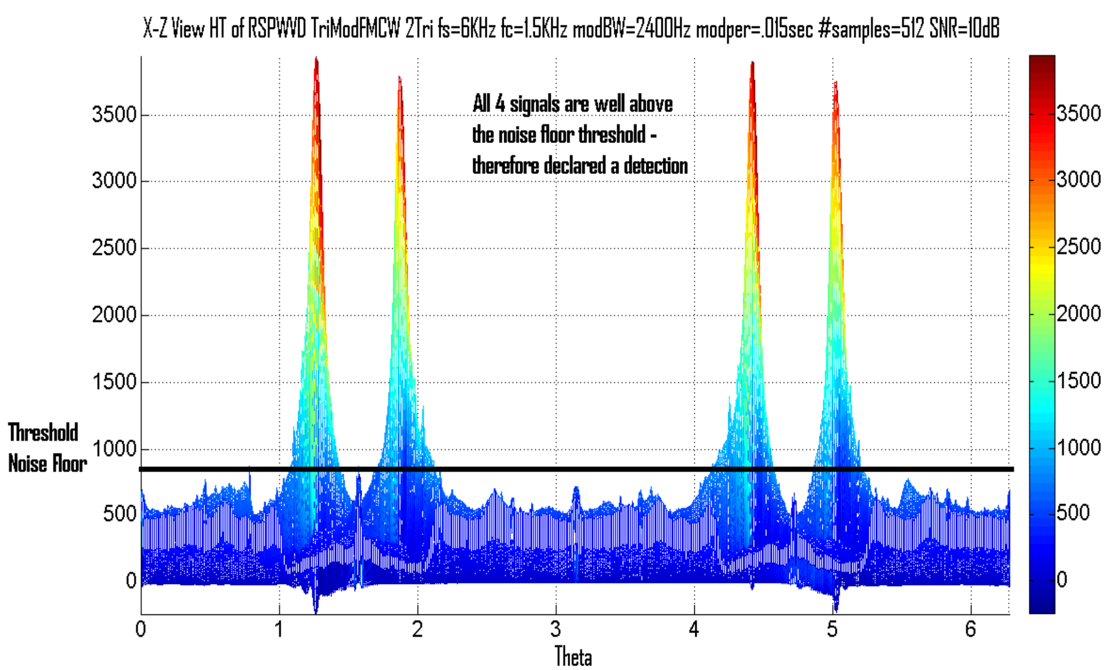

Figure 1 : Percent detection (Hough transform). This plot is a theta-intensity (x-z view) of the HT of an RSPWVD (512 samples, SNR=10dB). Signal declared a (visual) detection because at least a portion of each of the signal components exceeded the noise floor threshold.

TF: percent of time signal was detected - signal was declared a detection if any portion of each of the signal components (4 chirp components for triangular modulated FMCW, and 4 or 8 signal components for FSK) exceeded a set threshold (a certain percentage of the maximum intensity of the time-frequency representation).

Threshold percentages were determined based on visual detections of low SNR signals (lowest SNR at which the signal could be visually detected in the time-frequency representation) (see Figure 2).

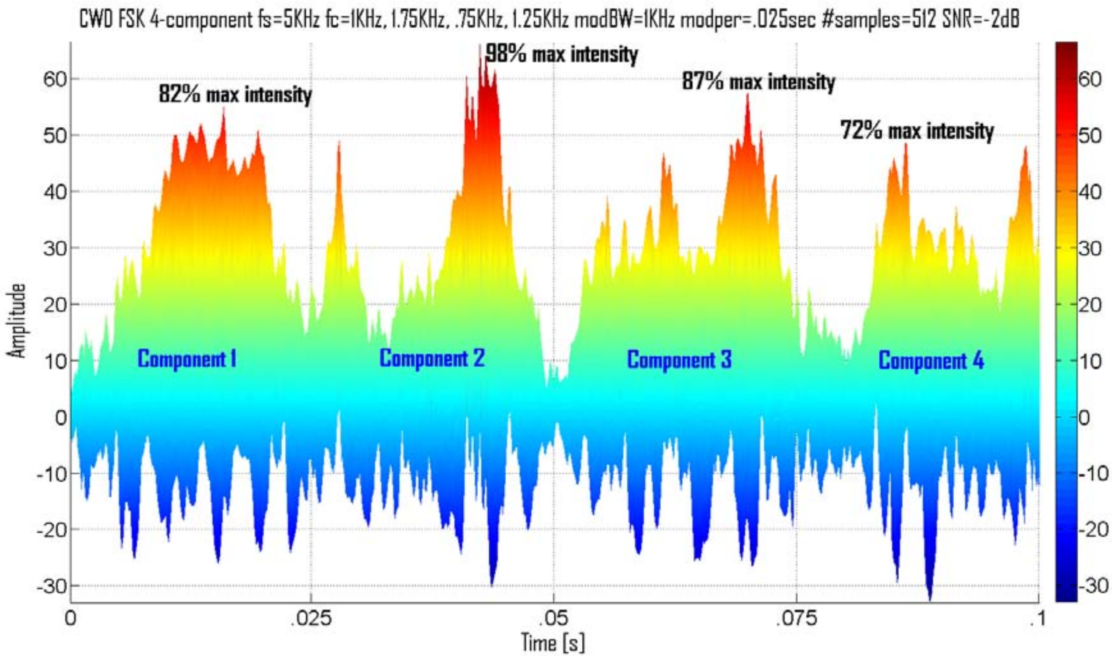

Figure 2 : Threshold percentage determination. This plot is an amplitude vs. time (x-z view) of CWD of FSK 4-component signal (512 samples, SNR= -2dB). For visually detected low SNR plots (like this one), the percent of max intensity for the peak z-value of each of the signal components was noted (here 82%, 98%, 87%, 72%), and the lowest of these 4 values was recorded (72%). Ten test runs were performed for each time-frequency analysis tool, for each of the 4 waveforms. The average of these recorded low values was determined and then assigned as the threshold for that particular time-frequency analysis tool. Note - the threshold for CWD is 70%.

Thresholds were assigned as follows: CWD (70%); spectrogram (60%); scalogram, WVD (4-component FSK) (50%); WVD (triangular modulated FMCW) (35%); WVD (8-component FSK) (20%).

For percent detection determination, these threshold values were included in the time-frequency plot algorithms so that the thresholds could be applied automatically during the plotting process. From the threshold plot, the signal was declared a detection if any portion of each of the signal components was visible (see Figure 3).

Global Journal of Researches in Engineering (J) Volume XV Issue VI Version I Year 2015

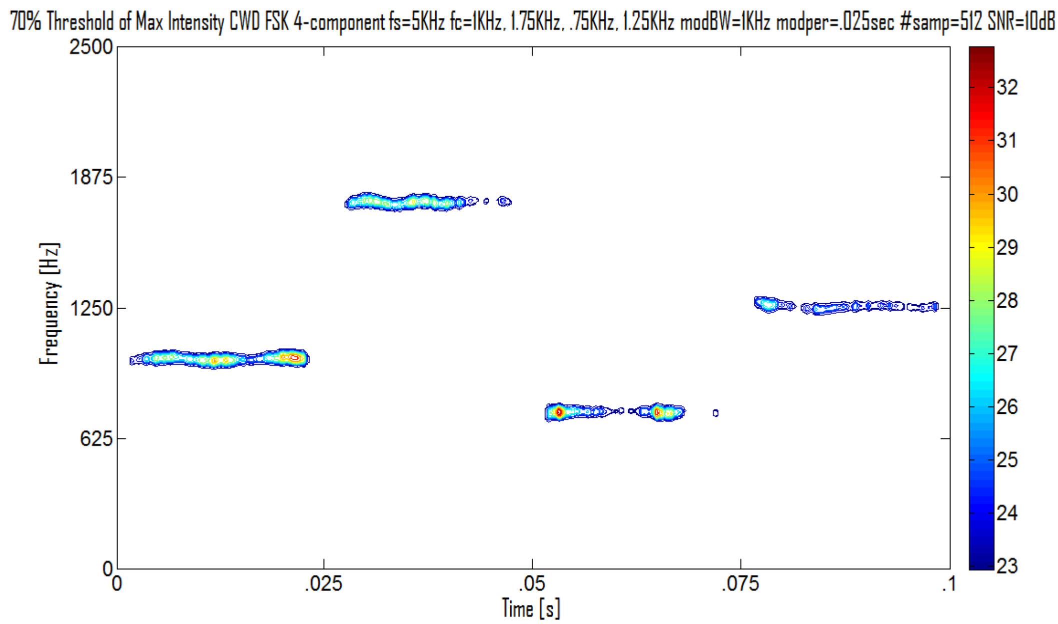

Figure 3 : Percent detection (time-frequency). CWD of 4-component FSK (512 samples, SNR=10dB) with threshold value automatically set to 70%. From this threshold plot, the signal was declared a (visual) detection because at least a portion of each of the 4 FSK signal components was visible.

Automatically applying a threshold value to the time-frequency plot algorithms for percent detection determination can be seen as a first step towards the future work of automating the metrics extraction process.

b) Cross-term false positives (XFPs)

The number of cross-terms that were wrongly declared as signal detections. For the time-frequency representation, the XFP detection criteria is the same as the time-frequency signal detection criteria listed in the percent detection section above. For the HT, the XFP detection criteria is the same as the HT signal detection criteria listed in the percent detection section above. Figure 4 shows a WVD plot with 4 true signals and 6 cross-terms, all 6 of which were XFPs.

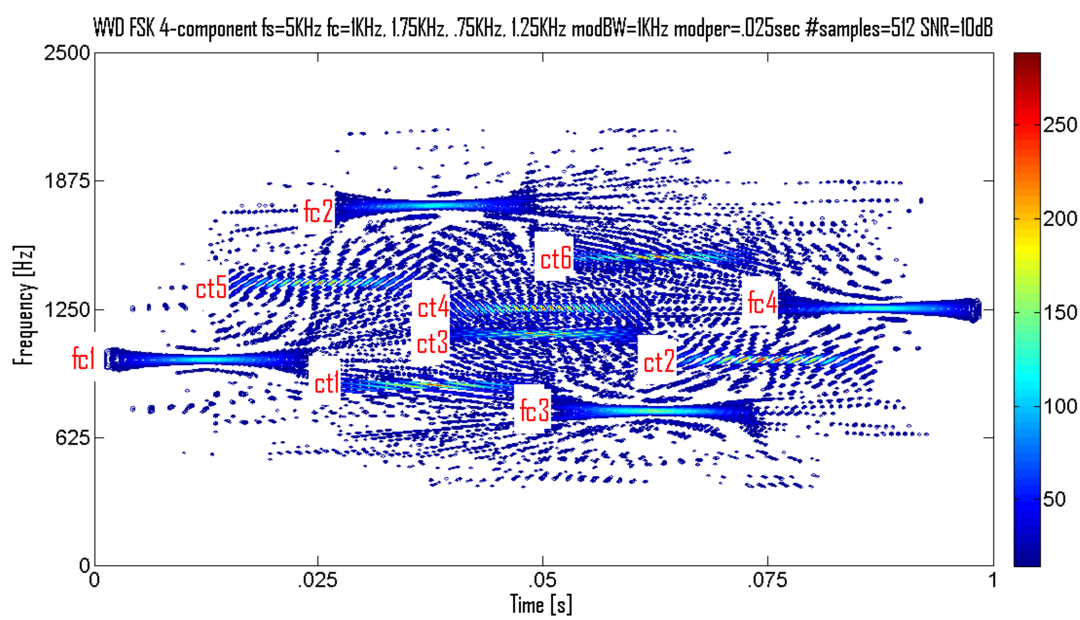

Figure 4 : Example of cross-term false positives (XFPs). WVD of a 4-component FSK signal at SNR=10dB (512 samples). There are 4 true signals (fc1=1KHz, fc2=1.75KHz, fc3=0.75KHz, fc4=1.25KHz) and 6 XFPs (cross-terms that were wrongly declared as signal detections because they passed the signal detection criteria listed in the percent detection section above) (ct1=0.875KHz, ct2=1KHz, ct3=1.125KHz, ct4=1.25KHz, ct5=1.375KHz, ct6=1.5KHz).

c) *Chirp rate*

HT: $chirprate = (-\tan\theta)\left(\frac{\max\ valueofY\ -axisofTFplot}{\max\ valueofX\ -axis\ ofTFplot}\right)$ – (for Task 1 and Task2 only).

TF: (modulation bandwidth/modulation period) – (for Task 1 and Task 2 only).

d) *Lowest detectable SNR*

HT: the lowest SNR level for which each signal component exceeded the noise floor threshold (see Figure 5).

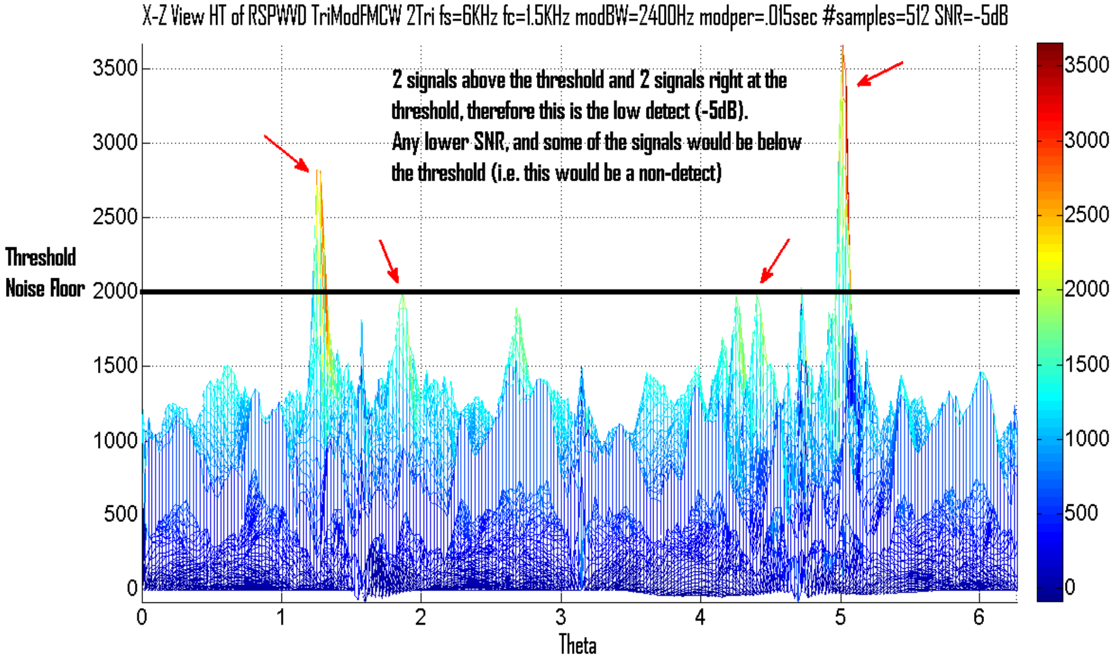

Figure 5 : Lowest detectable SNR (Hough transform). This plot is a theta-intensity (x-z view) of the HT of an RSPWVD (512 samples, SNR=-5dB). Signal declared a (visual) detection because at least a portion of each of the signal components exceeded the noise floor threshold. For this case, any lower SNR would have been a non-detect. Compare to Figure 1, which is the same plot, except that it has an SNR level equal to 10dB.

TF: the lowest SNR level at which at least a portion of each of the signal components exceeded the set threshold listed in the percent detection section above.

For lowest detectable SNR determination, these threshold values were included in the time-frequency plot algorithms so that the thresholds could be applied automatically during the plotting process. From the threshold plot, the signal was declared a detection if any portion of each of the signal components was visible. The lowest SNR level for which the signal was declared a detection is the lowest detectable SNR (see Figure 6).

Global Journal of Researches in Engineering (J) Volume XV Issue VI Version I Year 2015

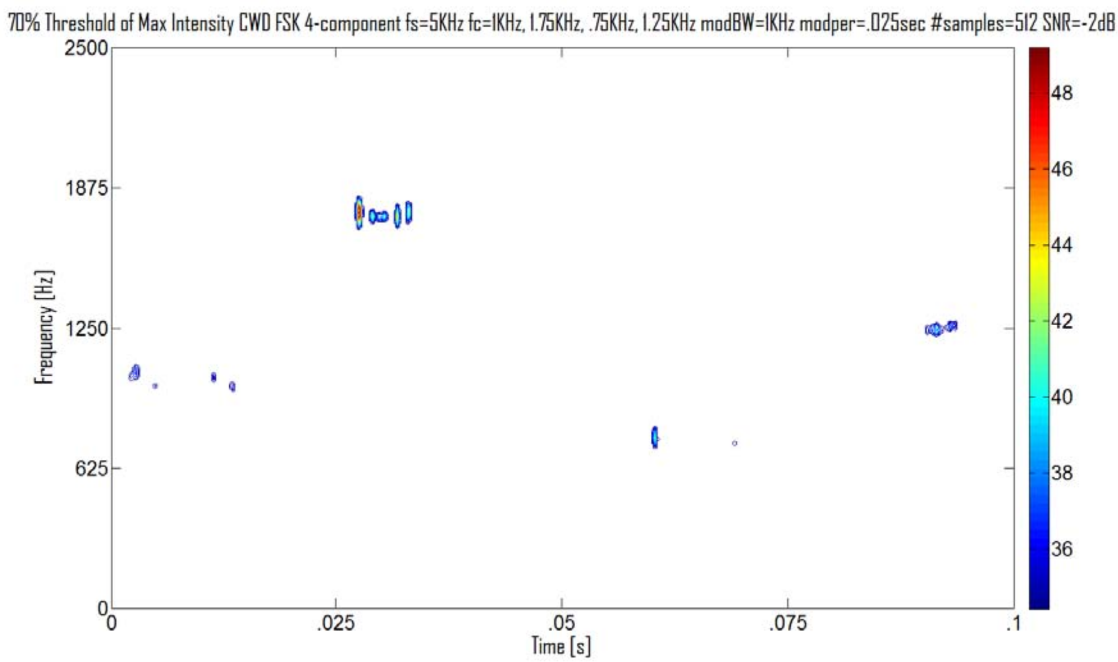

Figure 6 : Lowest detectable SNR (time-frequency). CWD of 4-component FSK (512 samples, SNR=-2dB) with threshold value automatically set to 70%. From this threshold plot, the signal was declared a (visual) detection because at least a portion of each of the 4 FSK signal components was visible. For this case, any lower SNR would have been a non-detect. Compare to Figure 3, which is the same plot, except that it has an SNR level equal to 10dB.

Automatically applying a threshold value to the time-frequency plot algorithms for the determination of the lowest detectable SNR can be seen as a first step towards the future work of automating the metrics extraction process.

The data from all 25 runs for each test was used to produce the mean, standard deviation, variance, actual, error, and percent error for each of these metrics listed above.

The metrics from the classical time-frequency analysis techniques were then compared to the metrics from the Hough transform. By and large, the Hough transform outperformed the classical time-frequency analysis techniques, as will be shown in the results section.

For Task 5, data from a CD was analyzed, with the only a priori knowledge being that the data contained an LPI radar signal in a low SNR environment (between -5dB and -10dB), and that the data was collected at a sampling frequency of 4GHz. The data (19 megabytes) was first processed using the Spectrogram (because it is the fastest time-frequency analysis tool). The signal was not visible in the Spectrogram time-frequency representation, due to low SNR. The data was then processed with the Hough transform of the Spectrogram, and the signal was detected, but had almost zero slope (like an FSK (tonal) signal). A MATLAB script was written which allowed for decimation of the Y-axis for the receiver IF bandwidth (~ 750MHz to 1250MHz), and then the data was re-processed with the Hough transform of the Spectrogram, this time for the purpose of determining if the signal had slope or if it was tonal. From the Hough transform plot it was observed that the signal had slope (i.e. was a chirp signal). The Hough transform plot allowed for not only detection of the chirp signal, but also for extraction of the chirp rate. A back-mapping from the Hough plot to the time-frequency representation was then performed. The signal was located in the time-frequency representation, and the modulation bandwidth and modulation period (and consequently the chirp rate) were extracted from the time-frequency representation. From these metrics, the type/source of the signal was identified. Additional details/results of Task 5 testing are addressed later in this chapter.

III. Results

Some of the graphical and statistical results of the testing are presented in this section.

Table 1 presents the overall test metrics (signal processing tool viewpoint) for the 4 time-frequency analysis techniques and the 2 Hough transform methods used in this testing.

Table 1 : Signal Processing Tool viewpoint of the overall test metrics (average percent error) for the 4 classical time-frequency analysis techniques (WVD, CWD, spectrogram, scalogram) along with their combined average (TF) and for the 2 Hough transform methods (WVD + HT, CWD + HT), along with their combined average (HT). The parameters extracted are listed in the left-hand column: chirp rate (cr), percent detection (% det), # of cross-term false positives (#XFP), lowest detectable SNR (low snr).

params	wvd	cwd	spectro	scalo	TF	wvd+ht	cwd+ht	HT
cr	5.29%	11.49%	16.25%	28.5%	15.4%	5.40%	2.74%	4.07%
% det	94.6%	92.5%	96.4%	90.4%	93.4%	100%	98.7%	99.4%
# XFP	25	0	0	0	25	4	4	8
low snr	-2db	-2.4db	-3db	-2.8db	-2.5db	-3db	-4.4db	-3.7db

From Table 1, the WVD had the best percent error of chirp rate (5.29%) of any of the classical time-frequency analysis tools, but performed the poorest out of all of the 6 signal processing techniques in the areas of number of cross-term false positives (25) and low SNR (-2dB). Figure 7(left-hand side) shows the cross-term interference problem that the WVD has.

The CWD performed 'middle-of-the-road' in every category (cr=11.49%; % det=92.5%; #XFP=0; low snr= -2.4dB) , as compared to the other classical time-frequency analysis techniques.

The spectrogram had the best low SNR (-3dB) and percent detection (96.4%) of the classical time-frequency analysis techniques, but had a poor percent error of chirp rate (16.25%).

The scalogram had the worst percent detection (90.4%) and percent error of chirp rate (28.5%) of the classical time-frequency analysis techniques, but did well in low SNR (-2.6dB).

The WVD + HT had a good percent error of chirp rate (5.40%) that was on par with that of the WVD (5.29%), and also had the best percent detection (100%) of all the 6 signal processing techniques. In addition, the WVD + HT had a low SNR value (-3dB) that equaled the best low SNR value of the classical time-frequency analysis techniques (spectrogram), and its number of cross-term false positives (4) was lower thanthat of the WVD (25) (see Figure 7 for comparison).

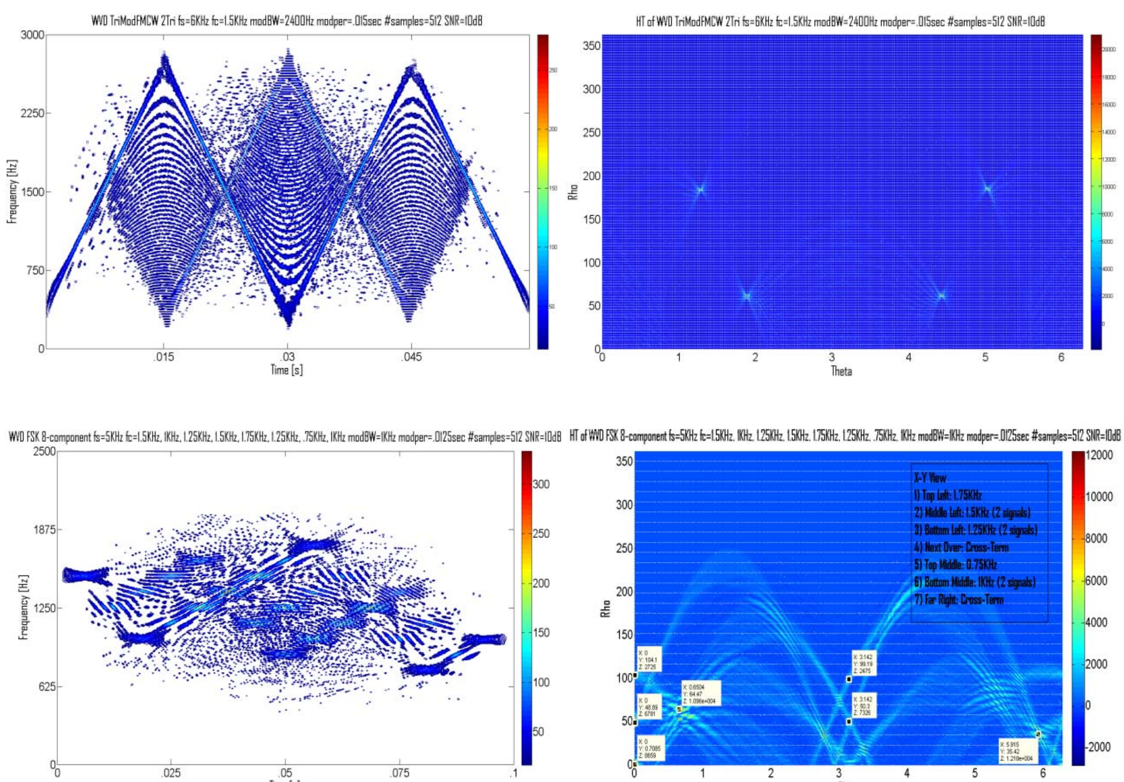

Figure 7 : Cross-term comparison between classical time-frequency analysis techniques (left) and the Hough transform (right). Top left: WVD of a triangular modulated FMCW signal (512 samples, SNR=10dB) (left). Top right: the Hough transform of the WVD of a triangular modulated FMCW signal (512 samples, SNR=10dB). Bottom left: WVD of an FSK (8-component) signal (512 samples, SNR=10dB). Bottom right: the Hough transform of theWVD of an FSK (8-component) signal (512 samples, SNR=10dB). Upper 2 plots – the Hough transform (right) has

eliminated the cross-term interference that the WVD (left) displays, making it easier to see the signal (better readability) in the Hough transform plot (the four bright spots which represent the four legs of the triangular modulated FMCW signal). The WVD appears to have another triangle signal between the outer two triangle signals. Lower 2 plots - In the WVD plot (left) there are 8 signal components and 9 cross-term components that appear to be signal components, all melded in together with one another. The 8 signal components are located at 5 distinct frequencies (one at 0.75KHz, two at 1KHz, two at 1.25KHz, two at 1.5KHz, and one at 1.75KHz). In the Hough transform plot (right) there are 8 signal components (located at 5 different frequencies (3 on the left-hand side of the plot and 2 in the middle of the plot)) plus 2 cross-term components, clearly separated from the signal components. The Hough transform plot makes it easier to see the signal components (better readability) as compared to the WVD plot.

The CWD + HT performed the best of all the 6 signal processing techniques in the areas of percent error of chirp rate (2.74%) and low SNR (-4.4dB) (see figure 8 (right-hand side)). It also performed very well for percent detection (98.7%).

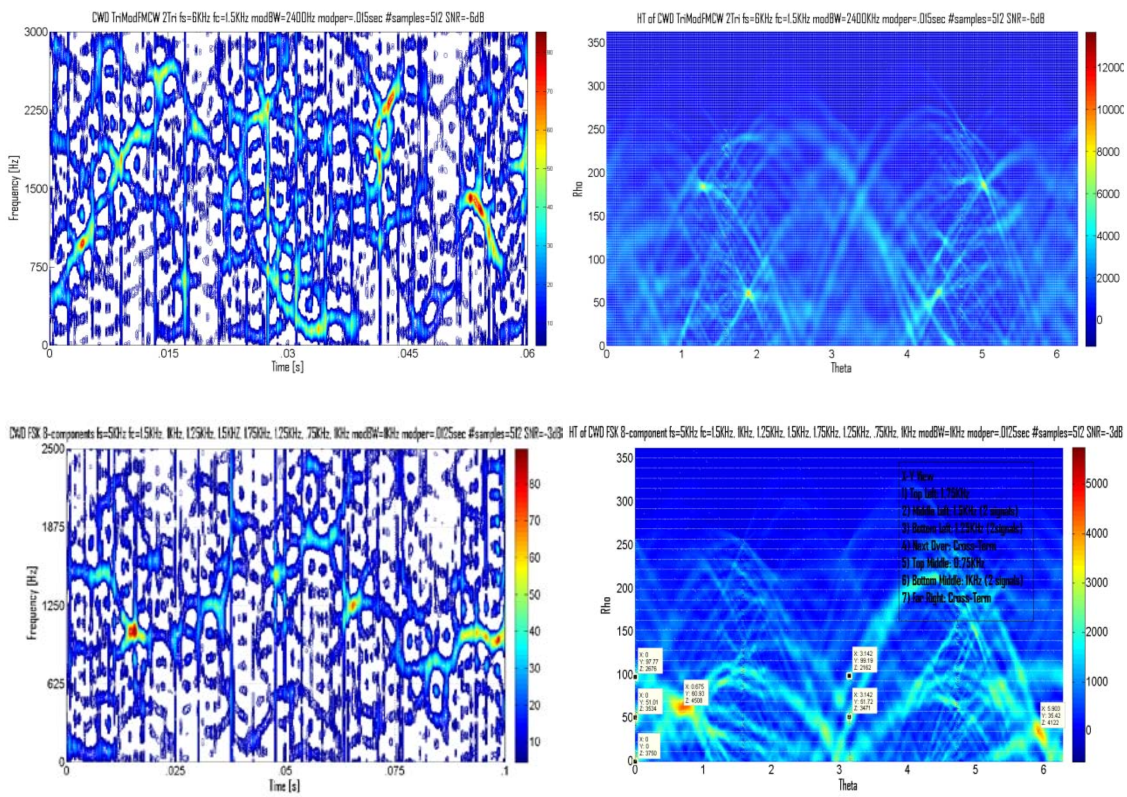

Figure 8 : Low SNR comparison between classical time-frequency analysis techniques (left) and the Hough transform (right). Top left: CWD of a triangular modulated FMCW signal (512 samples, SNR=-6dB) (left). Top right: the Hough transform of the CWD of a triangular modulated FMCW signal (512 samples, SNR=-6dB). Bottom left: CWD of an FSK (8-component) signal (512 samples, SNR=-3dB). Bottom right: the Hough transform of the CWD of an FSK (8-component) signal (512 samples, SNR=-3dB). Upper 2 plots - Though the signal is not visible in the CWD plot (left) (due to the low SNR (-6dB)), the four bright spots that represent the four legs of the triangular modulated FMCW signal are clearly seen in the Hough transform of the CWD plot (right). Each bright spot has a unique rho and theta value that can be used to back-map to the time-frequency representation (here CWD) and find the location of the 4 (non-visible) chirps that make up the triangular modulated FMCW signal. Lower 2 plots - Though the signal components are not visible in the CWD plot (due to the low SNR (-3dB)), the 5 bright spots (3 on the left and 2 in the middle) corresponding to the 5 different frequencies of the 8 FSK components are clearly visible in the Hough transform of the CWD plot (as are 2 cross-term components). The Hough transform does a good job of detecting the signal components and separating the signal components from the cross-term components, all in a low SNR environment.

Overall from Table 1, the Hough transform methods outperformed the classical time-frequency analysis techniques in percent error of chirp rate (4.07% to 15.4%), percent detection (99.4% to 93.4%), number of cross-term false positives (8 to 25), and low SNR (-3.7dB to -2.5dB).

Table 2 presents the overall test metrics (SNR viewpoint) for the testing performed in this paper.

Table 2 : SNR viewpoint of overall test metrics (average percent error) for the classical time-frequency analysis techniques (TF) and for the Hough transform methods (HT) for SNR=10dB, 0dB, and lowest detectable SNR (low SNR). The parameters extracted are listed in the left-hand column: chirp rate (cr), percent detection (% det), number of cross-term false positives (#XFP).

params	TF 10dB	TF 0dB	TF low snr	HT 10dB	HT 0dB	HT low snr
cr	13.73%	14.51%	17.04%	4.0%	6.23%	3.24%
% det	100%	82.4%	N/A	100%	98.7%	N/A
# XFP	21	2	2	2	0	4

Table 2 shows that the percent error of chirp rate and percent detection tended to worsen with lowering SNR values (see Figure 9) for both the classical time-frequency analysis techniques and the Hough transform (except for HT low SNR). The XFP numbers in Table 2 are representative of the fact that, due to computational complexity, there was no WVD testing accomplished at lower than 10dB (except for the 256 sample cases).

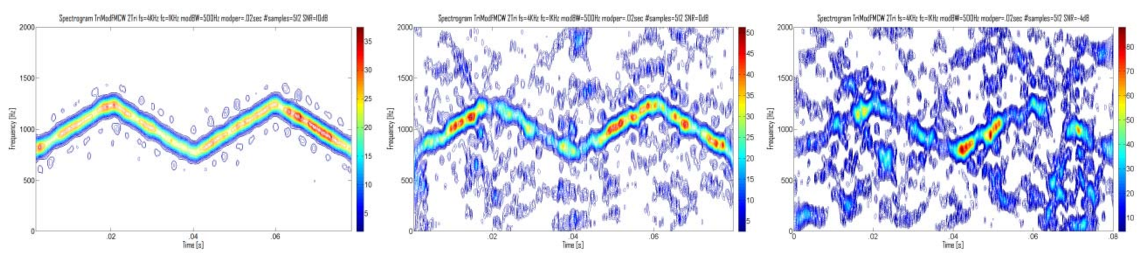

Figure 9 : Readability degradation due to reduction in SNR. Spectrogram, triangular modulated FMCW, modulation bandwidth=500Hz, 512 samples. SNR=10dB (left), 0dB (center), -4dB (left). Readability degrades as SNR decreases, negatively affecting the accuracy of the metrics extracted, as per Table 2.

Table 3 presents the overall test metrics (Task 1, 2, 3, and 4 view point) for the testing performed in this paper.

Table 3 : Task 1, 2, 3, and 4 viewpoint of overall test metrics (average percent error) for the classical time-frequency analysis techniques (TF) and for the Hough transform (HT). Task1=triangular modulated FMCW signal (modulation bandwidth=500Hz), Task2=triangular modulated FMCW signal (modulation bandwidth=2400Hz), Task 3=FSK (4-component) signal, Task 4=FSK (8-component) signal. The parameters extracted are listed in the left-hand column: chirp rate (cr), percent detection (% det), number of cross-term false positives (#XFP), lowest detectable SNR (low snr).

params	TF Task1	TF Task2	TF Task3	TFTask4	HTTask1	HTTask2	HTTask3	HTTask4
cr	12.09%	5.47%	N/A	N/A	3.68%	0.31%	N/A	N/A
% det	88%	93.7%	100%	100%	99.27%	100%	99.27%	100.0%
# XFP	8	2	6	9	0	0	4	4
low snr	-2.8db	-3.3db	-2.67db	-1.67db	-4.4db	-6.0db	-3.5db	-3.5db

Table 3 shows that the percent error of chirp rate, percent detection, and low SNR were all better for Task 2 (triangular modulated FMCW, modulation bandwidth=2400Hz) than for Task 1 (triangular modulated FMCW, modulation bandwidth=500Hz) for both the classical time-frequency analysis techniques and the Hough transform (see Figure 10). Also, the low SNR was lower for Task 3 (4-component FSK signal) than for Task 4 (8-component FSK signal).

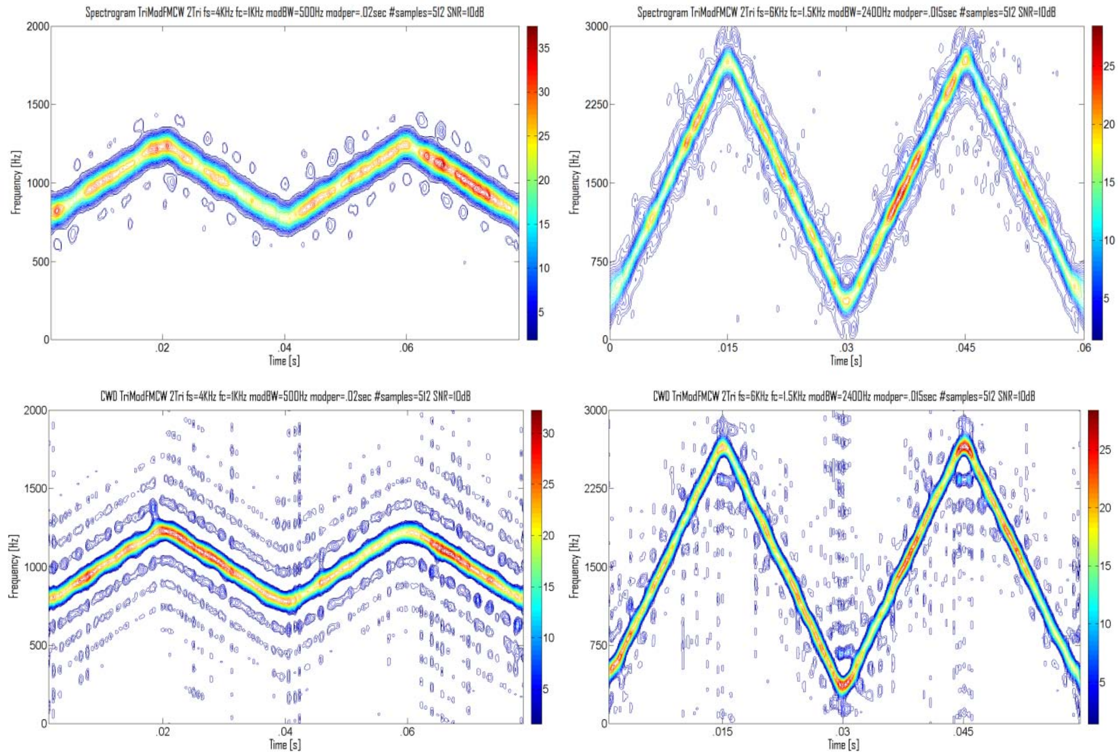

Figure 10 : Comparison between Task 1 (left) and Task 2 (right). The uppper two plots are both spectrogram plots of a triangular modulated FMCW signal (512 samples, SNR=10dB), Task 1 (modulation bandwidth=500Hz) is on the left and Task 2 (modulation bandwidth=2400Hz) is on the right. The lower two plots are CWD plots of the same signals. The Task 2 plots (right) have a larger modulation bandwidth than Task 1 plots, therefore the signals appear taller and more upright than the Task 1 signals.

Figure 11 shows a Spectrogram plot (left) of the area where the Task 5 real-world signal was located, though the signal was not visible in the Spectrogram plot (yellow area is in-band portion, and orange areas are out-of-band portion of band pass filter). The Hough transform of the Spectrogram (right) was performed, and the signal became visible, despite the low SNR environment (-5dB to -10dB). The Hough transform plot showed that the signal values were near theta=0 (or pi) and rho=0, which back-mapped to a nearly flat signal (i.e. tone) which was located near the center (frequency-wise) of the time-frequency representation. For this case, either the signal was a tonal (perhaps an FSK component), or the signal was a chirp; but because the bandwidth of the Spectrogram was so wide (2GHz) compared to the modulation bandwidth of the chirp, the chirp signal appeared 'flat'. For this case, the bandwidth of the Spectrogram needed to be reduced so that the slope of the signal (given that it is a chirp) would become apparent.

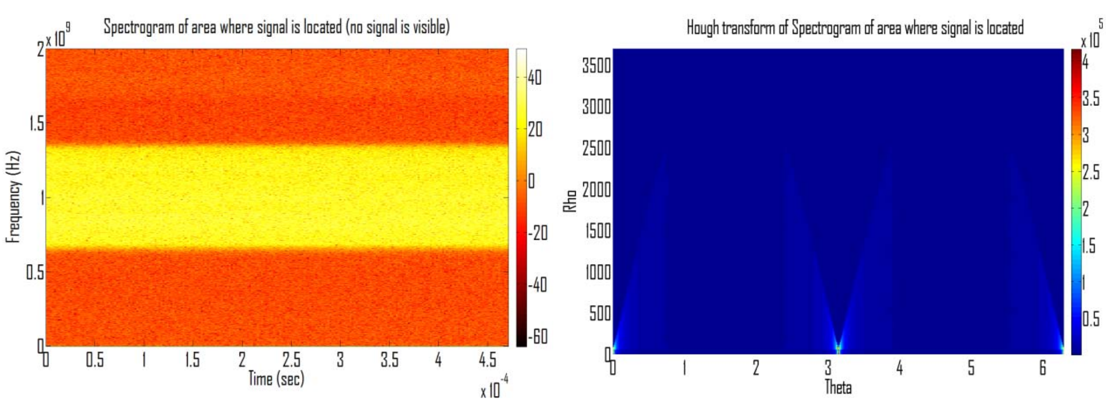

Figure 11 : Spectrogram (left) and Hough transform of Spectrogram (right) of area where Task 5 real-world signal was located. Signal was not visible in the spectrogram, but was visible in the Hough transform, due to the Hough transform's ability to extract signals from low SNR environments.

To investigate this further, a MATLAB script was utilized that that allowed for 'zooming-in' on the receiver IF bandwidth (representing the yellow portion of the Spectrogram in Figure 11 (~750MHz to 1250MHz)) (Y-axis zoom-in only). The data was processed again using the Hough transform of the Spectrogram (Figure 12). The signal appeared at theta=2.872 and rho=228.8, which indicatedthat the signal was indeed a chirp signal, with a chirp rate of

$$chirprate = (-\tan\theta)\left(\frac{\max valueofY - axisofTFplot}{\max valueofX - axis\,ofTFplot}\right)$$

or (-tan (2.872*57.3)(500MHz/471usec) = 0.28MHz/usec.

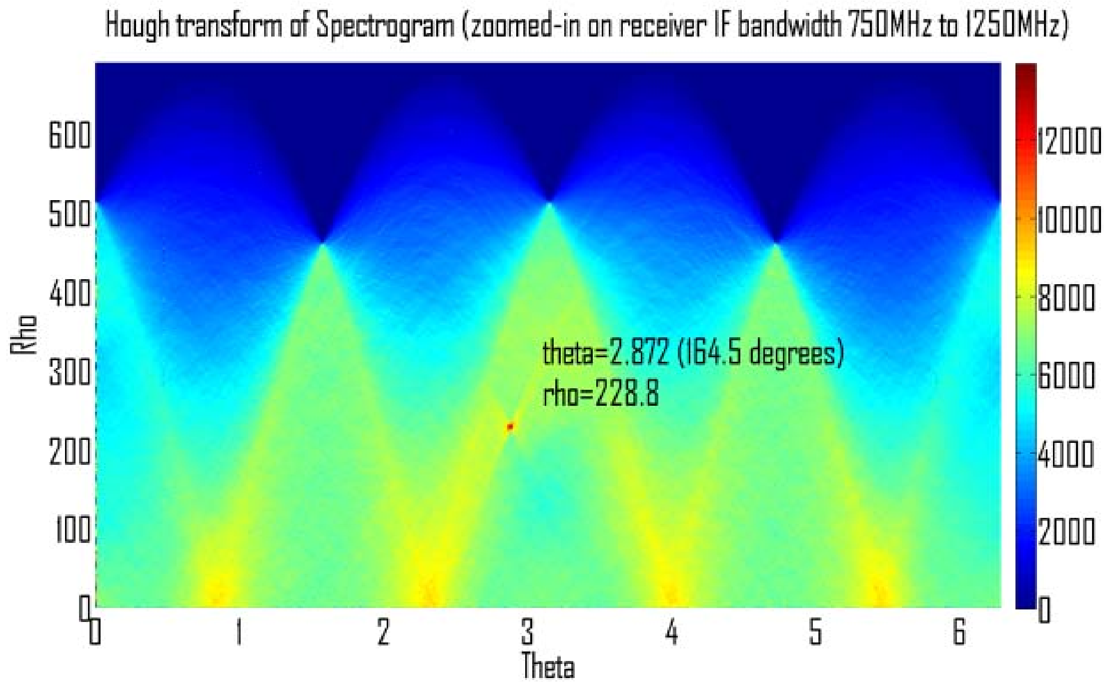

Figure 12 : Hough transform of Spectrogram (zoomed-in on receiver IF bandwidth (~750MHz to 1250MHz)) of area where Task 5 real-world signal was located. Signal is clearly visible at theta=2.872 and rho=228.8

Using these theta and rho values, back-mapping was performed from the Hough transform to the time-frequency representation (Spectrogram), which allowed the signal to be located (see Figure 13).

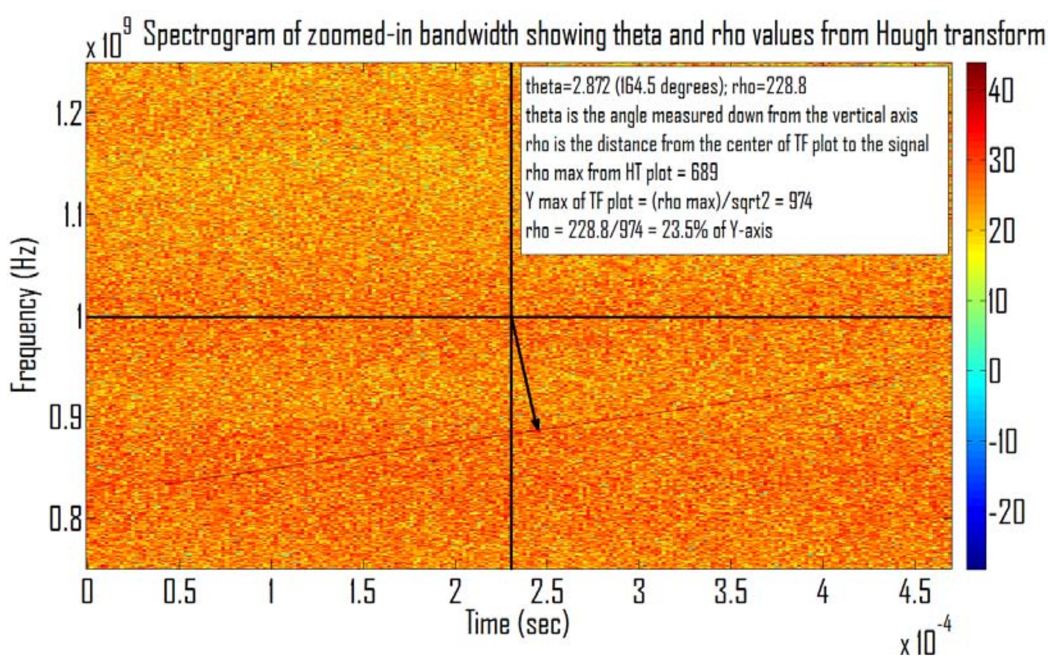

Figure 13 : Spectrogram (zoomed-in on receiver IF bandwidth (~750MHz to 1250MHz)). Shows how the Hough transform theta and rho values back-map to the time-frequency representation for signal location.

Once the chirp signal was detected in the Spectrogram, the modulation bandwidth (103MHz) and modulation period (389.34usec) metrics were extracted. The chirp rate (modulation bandwidth/modulation period) was then calculated to be 0.264 MHz/usec (very close to the chirp rate of 0.28MHz/usec obtained from the Hough transform plot).

Based on these parameters, it was determined that the signal was the front-end chirp of a particular LPI radar device, which was confirmed by the personnel who supplied the CD for testing.

IV. Discussion

This section of the paper will elaborate on the results from the previous section.

From Table 1 (signal processing tool viewpoint of overall test metrics), the performance of each of the 6 signal processing tools will be summarized, including strengths, weaknesses, and generic scenarios in which a particular tool might be used.

The WVD had the best percent error of chirp rate (5.29%) of all of the classical time-frequency analysis tools, but performed the poorest of all the 6 signal processing techniques in the areas of number of cross-term false positives (25) and low SNR (-2dB). Chirp rate can be seen as directly related to time-frequency localization. As per the methodology section, chirp rate is proportional to the modulation bandwidth. Since modulation bandwidth is a measure from the highest frequency value of a signal to the lowest frequency value of a signal, then the 'thinner' the signal (i.e. good time-frequency localization) the more accurate the modulation bandwidth (and therefore the more accurate the chirp rate), and the 'thicker' the signal (i.e. poor time-frequency localization) the less accurate the modulation bandwidth (and therefore the less accurate the chirp rate). Based on this, it can be said that the WVD's excellent chirp rate is due to its excellent time-frequency localization. This can be attributed to the fact that the WVD exhibits the highest signal energy concentration in the time-frequency plane [GUL07], [PAC09] and is totally concentrated along the instantaneous frequency [CIR08], [GUA06]. The WVD's cross-term interference problem, which is well-known [GUL07], makes it very difficult to see the actual signal [DEL02], [GUA06], [WON09], reducing the readability of the time-frequency distribution. Figure 7 clearly shows the cross-term interference problem that the WVD has. The cross-terms produced a false positive (XFP) triangle in the middle of the two-triangle signal (upper-left plot), and also produced 9 XFPs in the FSK 8-component signal (lower-left plot). Cross-terms are located half-way between signal components [DEL02], [WON09]. Though the WVD is highly concentrated in time and frequency, it is also highly non-linear and non-local, and is therefore very sensitive to noise [AUG95], [FLA03], which accounts for its poor low SNR performance (-2dB). The WVD might be a good tool to use if excellent chirp rate (time-frequency localization) is a requirement, but readability and low SNR environments are not an issue, such as in a scenario where off-line analysis is performed, without any time constraints (because of the WVD's slow plot time). The readability issue can be alleviated if a single-component signal is used, which would eliminate the cross-term interference, but which is unrealistic for LPI radar signals.

The CWD performed 'middle-of-the-road' in every category, as compared to the other classical time-frequency analysis techniques. Its decent performance for percent error of chirp rate (11.49%) (time-frequency localization) can be attributed to the fact that the CWD is part of the Cohen's class of time-frequency distributions, which use a smoothing kernel to smooth out cross-term interference, but at the expense of time-frequency localization [CHO89], [WIL92]. In this sense, the CWD is seen as a mid-point between the WVD (good localization, poor cross-term interference) and the spectrogram (poor localization, good cross-term interference). The fact that it doesn't smooth out all of the cross-term interference allows for decent localization (and therefore decent chirp rate). The CWD might be used in a scenario where above average localization (chirp rate) is required (i.e. somewhere between the WVD and the spectrogram). The goal of such a scenario would be to obtain above average signal metrics in a short amount of time (due to the CWD's fairly quick plot time).

The spectrogram had the best low SNR (-3dB) and percent detection (96.4%) of the classical time-frequency analysis techniques, but had a poor percent error of chirp rate (16.25%). It is known that the spectrogram suffers in time-frequency localization (and therefore chirp rate)[ISI96], [COH95], [HLA92]. The results of these 3 metrics can be attributed to the spectrogram's extreme reduction of cross-term interference, which accounts for good low SNR, and percent detection, but at the expense of poor time-frequency localization (chirp rate). The spectrogram might be used in a scenario where a short plot time is necessary (since it is the fastest time-frequency technique), in a fairly low SNR environment, and where time-frequency localization (chirp rate) is not an issue. Such a scenario might be a 'quick and dirty' check to see if a signal is present, without precise extraction of its parameters.

The scalogram had the worst percent detection (90.4%) and percent error of chirp rate (28.5%) of the classical time-frequency analysis techniques, but did well in low SNR (-2.8dB). The scalogram suppresses almost all cross-terms [GRI07], [LAR92], accounting for its good low SNR performance. Because of this cross-term reduction, it is surprising that the scalogram did not perform better in the area of percent detection. This could be due to its bad time-frequency localization (chirp rate), or to the fact that a wavelet/scalogram performs better on signals that change rapidly in frequency over time, vice the triangular modulated FMCW and FSK signals used in this paper. Like the spectrogram, the scalogram might be used in a scenario where short plot time is necessary (the scalogram has a very fast plot time), in a fairly low SNR environment, and where time-frequency localization (chirp rate) is not an issue, or in a scenario that detects/analyzes signals that change rapidly in frequency over time.

The WVD + HT and the CWD + HT both had good percent error of chirp rates (5.40%/2.74%), that were on par with or better than that of the WVD (5.29%). In addition, the WVD + HT and the CWD + HT both had good percent detections (100%/98.7%) and low SNRs (-3dB/-4.4dB) (see Figure 8). In the presence of noise, the integration carried out by the Hough transform produces an improvement in SNR [INC07], [YAS06], [NIK08]. The WVD + HT and the CWD + HT both had a lower number of cross-term false positives (4/4) than did the WVD (25) (see Figures 7 and 8 for comparison).Since cross-terms have amplitude modulation, the integration implicit in the Hough transform reduces the cross-terms, while the useful contributions, which are always positive, are correctly integrated [TOR07], [BAR95].

Overall from Table 1, the Hough transform methods outperformed the classical time-frequency analysis techniques in percent error of chirp rate (4.07% to 15.4%), percent detection (99.4% to 93.4%), number of cross-term false positives (8 to 25), and low SNR (-3.7dB to -2.5dB).

From Table 2, it was seen that in general, the percent error of chirp rate and percent detection metrics tended to worsen with lowering SNR values, for both the classical time-frequency analysis techniques and the Hough transform (except for HT low SNR). Figure 9shows how readability is degraded as the SNR level is lowered. It is noted that the for the chirp rate metrics, the classical time-frequency analysis techniques experienced a 17.4% degradation of metrics while going from 0dB to low SNR, while the HT experienced a 48% improvement in metrics while going from 0dB to low SNR. This highlights the classical time-frequency analysis techniques mediocre performance in a low SNR environment, and also highlights the Hough transform's robust performance in a low SNR environment. This translates to improved readability of the Hough transform plot over the classical time-frequency analysis representation in low SNR environments. As noted previously, the XFPs in Table 2 are representative of the fact that, due to computational complexity, there was no WVD testing accomplished at lower than 10dB (except for the 256 sample cases). Had testing been able to be accomplished at lower than 10dB SNR levels for the 512 sample cases, the XFP numbers would have likely increased as the SNR level decreased. Table 2 shows by-and-large that the Hough transform's metrics were more accurate than the classical time-frequency analysis techniques' metrics at every SNR level.

From Table 3, it was seen that the percent error of chirp rate, percent detection, and low SNR are all better for Task 2 (triangular modulated FMCW, modulation bandwidth=2400Hz) than for Task 1 (triangular modulated FMCW, modulation bandwidth= 500Hz) for both the classical time-frequency analysis techniques and the Hough transform. As per Figure 10, the modulation bandwidth is a measure from the highest frequency point of a signal to the lowest frequency point of a signal. Therefore, the 'thickness' of a signal will affect the modulation bandwidth measurement of a 'shorter' signal (Task 1 – left-hand side of Figure 10)) more than that of a 'taller' signal (Task 2 – right-hand side of Figure 10)). Because of this, the modulation bandwidth percent error will be lower for Task 2 (the 'taller' signal) than for Task 1 (the 'shorter' signal). Since chirp rate is proportional to modulation bandwidth, then chirp rate percent error will be lower for Task 2 (the 'taller' signal) than for Task 1 (the 'shorter' signal). As mentioned previously, chirp rate is proportional to time-frequency localization; therefore time-frequency localization will be better for Task 2 than for Task1. Better time-frequency localization translates to better readability, which in turn makes for better percent detection and low SNR values, which accounts for Task 2 having better metrics for these 2 parameters than Task 1. For the Hough transform, the 'longer', 'tighter' signal of Task 2 translates to a 'higher' (greater accumulator value) and 'tighter' spike in the Hough transform plot. The 'higher' spike accounts for the better percent detection and low SNR values of Task 2, because the signal (spike) is that much higher than the noise floor. The 'tighter' signal makes for a more accurate theta value extraction, which in turn makes for a more accurate chirp rate (since chirp rate is proportional to theta per the methodology section). It was also noted that for the classical time-frequency analysis techniques, the low SNR value was lower for Task 3 (4-component FSK signal) than for Task 4 (8-component FSK signal). This may be due to the fact that the Task 3 signal has only 4 components, each of which is twice as long as the Task 4 signal's 8-components. This means that at low SNR levels, the Task 3 signal has a better chance of at least a portion of each of its 4 (longer) signal components exceeding the low SNR threshold than does the Task 4 signal with its 8 (shorter) components. Table 3 shows by-and-large that the Hough transform's metrics were more accurate than the classical time-frequency analysis techniques' metrics for each of the 4 Tasks.

Figure 11 shows that the Spectrogram, though the fastest classical time-frequency analysis technique

[HLA92], did not have the ability to detect the signal in a low SNR environment (-5dB to -10dB). However, in the presence of noise, the integration carried out by the Hough transform produces an improvement in SNR [INC07], [YAS06], [NIK08], and therefore the Hough transform was able to 'dig' the signal out of the noise. The ability to back-map from the Hough transform to the time-frequency representation, based on theta and rho values of the signal, allowed for a quick deduction that the signal (in the time-frequency representation) was nearly 'flat' and that it was located near the middle of the plot (frequency-wise). The ability to zoom-in (Y direction only) on the receiver IF bandwidth (the yellow portion of the Spectrogram of Figure 11) and then perform a Hough transform of the Spectrogram (Figure 12) made possible the detection and chirp rate extraction (0.28MHz/usec) of the signal, and also the determination that the signal was a chirp and not a tone. Back-mapping once again allowed for the signal location to be found in the time-frequency representation. Once the modulation bandwidth (103MHz) and modulation period (389.34usec) values were extracted, and the chirp rate (modulation bandwidth/modulation period) was calculated (0.264MHz/usec, very close to the Hough transform calculated value of 0.28MHz/usec), then identification of the LPI radar device that emitted the signal was straight-forward.

Recapping, the metrics data backs up the following introductory assumptions:

The classical time-frequency analysis techniques are deficient in the areas of cross-term interference and mediocre performance in low SNR environments, making for poor readability and consequently, inaccurate detection and parameter extraction of LPI radar signals.

The Hough transform's qualities of cross-term reduction, separating signals from cross-terms, and good performance in low SNR environments make for better readability and consequently, for more accurate signal detection and parameter extraction of LPI radar signals.

V. Conclusions

It was noted that digital intercept receivers are currently moving away from Fourier-based analysis and towards classical time-frequency analysis techniques, such as the Wigner-Ville distribution, Choi-Williams distribution, spectrogram, and scalogram, for the purpose of analyzing low probability of intercept radar signals (e.g. triangular modulated FMCW and FSK). Though these classical time-frequency techniques are an improvement over the Fourier-based analysis, it was shown through the testing plots that they suffer from a lack of readability, due to cross-term interference, and a mediocre performance in low SNR environments, as brought out in the discussion section of this chapter. It was shown through testing metrics that this lack of readability led to inaccurate detection and parameter extraction of the LPI radar signals, which would undoubtedly make for a less informed (and therefore less safe) intercept receiver environment. Simulations were presented that compared time-frequency representations of the classical time-frequency techniques with those of the Hough transform. Two different triangular modulated FMCW LPI radar signals and two different FKS LPI radar signals (4-component and 8-component) were analyzed. The following metrics were used for evaluation of the analysis: percent error of chirp rate, percent detection, number of cross-term false positives, and lowest signal-to-noise ratio for signal detection. Experimental results demonstrated that the Hough transform's ability to suppress cross-term interference, separate signals from cross-terms, and perform well in the presence of noise did indeed lead to improved readability over the classical time-frequency analysis techniques, and consequently, provided more accurate signal detection and parameter extraction metrics (smaller percent error from true value) than the classical time-frequency analysis techniques. In summary, this paper provided evidence that the Hough transform has the potential to outperform the classical time-frequency analysis techniques. In addition, the Hough transform was utilized to detect, extract parameters, and properly identify a real-world LPI radar signal in a low signal-to-noise ratio environment where classical time-frequency analysis failed. Future plans include automation of the metrics extraction process, analysis of additional low probability of intercept radar waveforms of interest, and analysis of other real-world low probability of intercept radar signals utilizing more powerful computing platforms.

References Références Referencias

1. [AUG95] Auger, F., Flandrin, P., Improving the Readability of Time-Frequency and Time-Scale Representations by the Reassignment Method. IEEE Transactions on Signal Processing, 43(5):1068-1089, 1995.
2. [BAR92] Barbarossa, S., Zanalda, A., A Combined Wigner-Ville and Hough Transform for Cross-Terms Suppression and Optimal Detection and Parameter Estimation. ICASSP '92, Vol. 5, pp. 173-176, 1992.
3. [BAR95] Barbarossa, S., Analysis of Multicomponent LFM Signals by a Combined Wigner-Hough Transform. IEEE Transactions on Signal Processing, Vol. 43, No. 6, pp. 1511-1515, 1995.
4. [BEN05] Bennett, N., Saito, N., Using Edge Information in Time-Frequency Representations for Chirp Parameter Estimation. Applied Computational Harmonic Analysis, pp. 186-197, 2005.

5. [BOA03] Boashash, B., Time Frequency Signal Analysis and Processing: A Comprehensive Reference. Elsevier, Oxford, England, 2003.
6. [CHO89] Choi, H., Williams, W., Improved Time-Frequency Representation of Multicomponent Signals Using Exponential Kernels. IEEE Transactions on Acoustics, Speech, and Signal Processing. Vol. 37, pp. 862-871, June 1989.
7. [CIR08] Cirillo, L., Zoubir, A., Amin, M., Parameter Estimation for Locally Linear FM Signals Using a Time-Frequency Hough Transform. IEEE Transactions on Signal Processing, Vol. 56, No. 9, pp. 4162-4175, Sept. 2008.
8. [COH02] Cohen, L., The Wavelet Transform and Time-Frequency Analysis. in: Debnath, L., Wavelet Transforms and Signal Processing, Birkhauser, pp. 3-22, 2002.
9. [COH95] Cohen, L., Time-Frequency Analysis. Prentice Hall, Upper Saddle River, NJ, 1995.
10. [DEL02] De Luigi, C., Moreau, E., Wigner-Ville and Polynomial Wigner-Ville Transforms in the Estimation of Nonlinear FM Signal Parameters. IEEE International Conference on Acoustics, Speech, and Signal Processing, Orlando, FL, Vol. 2, pp. 1433-1436, May 13-17, 2002.
11. [FLA03] Flandrin, P., Auger, F., Chassande-Mottin, E., Time-Frequency reassignment: From principles to algorithms, in Applications in Time-Frequency Signal Processing (A. Papandreou-Suppappola, ed.), ch. 5, pp. 179-203, CRC Press, 2003.
12. [GAL05] Galleani, L., Cohen, L., Noga, A., A Time-Frequency Approach to the Adjustable Bandwidth Concept. Digital Signal Processing, Vol. 16, Issue 5, pp. 454-467, Sept. 2006.
13. [GER09] Geroleo, F., Periodic Wigner-Ville Hough Transform for LFMCW Detection. Low Probability of Intercept ELINT/SIGINT Conference, Monterey, CA, November 17-19, 2009.
14. [GRI07] Grishin, Y., Janczak, D., Computer-Aided Methods of the LPI Radar Signal Detection and Classification. Proc. of SPIE Vol. 6937, pp. 1-5, 2007.
15. [GUA06] Guanghua, C., Shiwei, M., Tinghao, Q., Jian, W., Jialin, C., The Wigner-Ville Distribution and the Cross Wigner-Ville Distribution of Noisy Signals. Journal of Systems Engineering and Electronics, Vol. 19, Issue 5, pp. 1053-1057, August 2008.
16. [GUL07] Gulum, T., Autonomous Non-Linear Classifications of LPI Radar Signal Modulations. Thesis, Naval Postgraduate School, Monterey, CA, 2007.
17. [GUL08] Gulum, T., Pace, P., Cristi, R., Extraction of Polyphase Radar Modulation Parameters Using a Wigner-Ville Distribution-Radon Transform. IEEE International Conference on Acoustics, Speech, and Signal Processing, Las Vegas, NV, April 2008.
18. [HLA92] Hlawatsch, F., Boudreaux-Bartels, G.F., Linear and Quadratic Time-Frequency Signal Representations. IEEE Signal Processing Mag., Vol. 9, No. 2, pp. 21-67, April 1992.
19. [INC07] Incer, I., Kaminsky, E., Performance of Chirp-Slope Keying with Joint Time-Frequency Detectors. Proc. of SPIE Vol. 6577, 6577OH, pp. 1-9, 2007.
20. [ISI96] Auger, F., Flandrin, P., Goncalves, P., Lemoine, O., Time-Frequency Toolbox Users Manual. Centre National de la Recherche Scientifique and Rice University, 1996.
21. [LAR92] Lari, F., Zakhor, A., Automatic Classification of Active Sonar Data Using Time-Frequency Transforms. Proceedings of IEEE-SP International Symposium on Time-Frequency and Time-Scale Analysis, Victoria, BC, pp. 21-24, Oct. 4-6, 1992.
22. [LIA09] Liang, Y., Zhang, L., Xing, M., Bao, Z., High-Speed Ground Moving Target Detection Research Using Triangular Modulation FMCW. Front. Electr. Electron. Eng., China, 4(2), pp. 127-133, 2009.
23. [MIL02] Milne, P., Pace, P., Wigner Distribution Detection and Analysis of FMCW and P-4 Polyphase LPI Waveforms. Proceedings of ICASSP, Orlando, FL, pp. 3944-3947, 2002.
24. [MIT01] Mitra, S., Digital Signal Processing, A Computer-Based Approach, Second Edition. McGraw-Hill, Boston, MA, 2001.
25. [NIK08] Nikolaev, D., Nikolaev, I., Karpenko, S., Nikolayev, P., Hough Transform: Underestimated Tool in the Computer Vision Field. 22nd European Conference on Modeling and Simulation, Nicosia, Cyprus, June 3-6, 2008.
26. [PAC09] Pace, P., Detecting and Classifying Low Probability of Intercept Radar. Artech House, Norwood, MA, 2009.
27. [STE96] Stephens, J., Advances in Signal Processing Technology for Electronic Warfare. IEEE AES Systems Magazine, pp. 31-38, November 1996.
28. [TOR07] Toronto, N., Morse, B., Ventura, D., Seppi, K., The Hough Transform's Implicit Bayesian Foundation. IEEE International Conference on Image Processing, Vol. 4, pp. IV-377 – IV-380, October 2007.
29. [UPP08] Upperman, T., ELINT Signal Processing Using Choi-Williams Distribution on Reconfigurable Computers for Detection and Classification of LPI Emitters. Thesis, Naval Postgraduate School, Monterey, CA, March 2008.
30. [WIL06] Wiley, R., ELINT: The Interception and Analysis of Radar Signals. Artech House, Norwood, MA, 2006.

31. [WIL92] Williams, W., Jeong, J., Reduced Interference Time-Frequency Distributions. Time-Frequency Signal Analysis: Methods and Applications (B. Boashash, ed.), Longman-Cheshire/Wiley, Melbourne/N.Y., 1992.
32. [WON09] Wong, K., Davidson, T., Abelkader, S., Detection of Low Probability of Intercept Radar Signals. Defence R&D Canada – Ottawa Contract Report 2009-142, September 2009.
33. [XIE08] Xie, C., Zhang, K., Feng, K., Guo, C., Xu, J., Target Detecting Based on Improved WVD-HT for Radio Frequency Interference to UWB-SAR. First International Conference on Intelligent Networks and Intelligent Systems, pp. 604-607, 2008.
34. [YAS06] Yasotharan, A., Thayaparan, T., Optimum Time-Frequency Distribution for Detecting a Discrete-Time Chirp Signal in Noise. IEE Proc.-Vis. Image Signal Process., Vol. 153, No. 2, pp. 132-140, April 2006.
35. [ZAI99] Zaino, J., Bassett, R., et al. An FPGA-Based Adaptive Computing Implementation of Chirp Signal Detection. RAAC, pp. 1-21, 1999.